Surface quality of laser rod end melted shape-memory Nitinol preforms

Yang Lu, Tim Radel
Bremer Institut für angewandte Strahltechnik GmbH, Klagenfurter Straße 5, 28359 Bremen

The shape-memory Nitinol as a nickel-titanium alloy is widely used in actuator and medical applications. However, the connection of a flange to the rod is a critical point. Therefore, laser rod end melting enables material accumulations to generate a preform at the end of a rod, followed by die forming, so that the flange can be generated. This process has been successfully applied on 1.4301 steel. This study is aimed to investigate laser rod end melting of shape-memory Nitinol regarding the resultant surface quality of the preforms. The results showed that spherical preforms could be generated without visible surface discoloration due to oxidation. By using different scan rates, different solidification conditions occurred which led to significantly different surface structures. These findings show that laser rod end melting can principally be applied on Nitinol to generate preforms for flanges whereby the surface quality depends on the solidification conditions.

1. Introduction

Nitinol is a nickel-titanium (NiTi) shape memory alloy (SMA) with two special properties, superelasticity and shape memory effect. These properties enable its application actuator and sensor, which have been widely used in automobile, aerospace, medical and electronic applications [1]. However, there is no standardized flange and shaft design of a Nitinol actuator that could easily integrated into mechanical design, and crimping and screwing are the alternative solution for the attachment of Nitinol actuator to the mechanical system [2]. Furthermore, Nitinol is a hard-to-machining material due to its high ductility and strong work hardening, requiring robust and reliable joining methods for SMA to design complex functional components rather than the conventional cold working [3].

In this case, a two-stage shaping process, so-called laser rod end melting, could serve as a solution. This process enables the fabrication of functional component including rod and flange design at its end. It consists of a laser melting of a preform and subsequent die forming [4]. In the laser melting stage, the end of rod is melted by a laser beam, which is transferred to the accumulated melt. The solidified melt maintains its spherical shape as preform. Subsequently, the preform is reshaped to the designed shape via a single cold die forming step [4]. Based on this, an intensive investigation was conducted on 1.4301 steel [5]. The main results showed that radiation strategies and composition of laser power and irradiation time play an important role in determining the preform volume. During the solidification, preform diameter affects the cooling time and dendritic solidified structure, especially secondary dendrite arm spacing, which influences the yield stress. Finally, the oversized preform compared to the die volume can be manufactured with fine surface structure [5].

Up to now, laser rod end melting has been successfully applied mainly on steels (1.4301 [5], 1.4310 [6]), which can be transferred to fabricate the Nitinol actuator with flange design. Considering the cooling effect of Nitinol melt, laser welding is the most used joining technique for NiTi alloys, and the relative phenomena have been intensively investigated [3]. The laser affected zone consists of fusion zone (FZ), heat affected zone (HAZ) and unaffected base material (BM), where a dendritic, planar or cellular microstructure or a combination of these can be found in the FZ of the NiTi laser welds [7]. It can be explained according to rapid solidification theory, by which temperature gradient G and growth rate of solid-liquid interface R determine morphology (by G/R) and size of the microstructure (by G×R, i.e. cooling rate) [8]. Specifically, decreasing G/R leads to increasing constitutional supercooling, by which solidification mode changes from planar to cellular, columnar dendritic and equiaxed dendritic in turn [8].

For laser welding of Nitinol to Nitinol, the microstructure investigations present coarse grains in the FZ and fine equiaxial crystals in the HAZ [9]. Close to the fusion line an epitaxial growth occurs, where the grain structure depends on the BM and laser parameter, which define the solidification conditions [3]. In addition, composition in the weld zone may vary slightly compared to the BM [9]. The Ni/Ti ratio in the FZ can vary as a result of the precipitation of Ni_3Ti, leading to a change of austenite-martensite transformation temperature [3]. Therefore, it is aimed to achieve only a minor change of transformation temperature in this region for the optimum functional performance.

Nevertheless, there are some potential defects and imperfections during fusion welding of Nitinol, such as cracks [9], voids [10], gas porosity [11] and embrittlement [11]. The solidification cracking can be explained by the formation of brittle Ti_2Ni phase during either rapid solidification of a Ti-rich NiTi-phases or Ni-rich NiTi-phases with oxygen atmosphere [12]. In addition, softening effect usually takes place in the generated HAZ and FZ, which is mainly attributed to precipitate dissolution, dislocation movement and grain coarsening [3]. Furthermore, laser-induced preferential evaporation of Ni leads to local changes of functional characteristics [7].

Based on the state of the research, two-stage laser rod end melting shows the potential to fabricate functional components of Nitinol, which may exhibit a better connection strength compared to the conventional mechanical joining method. This study is focused on the first stage of generation of preform and aimed to investigate laser rod end melting of shape-memory Nitinol regarding the resultant surface quality and microstructure of the preforms.

2. Methodology

2.1. Material and laser processing

Laser rod end melting of Nitinol was conducted with a continuous wave laser (YLR-100-AC, IPG Laser GmbH) with gaussian intensity distribution, wavelength of 1070 nm and a maximum laser power about 100 W. The studied Nitinol (SmartFlex05, SAES Getters S.p.A.) was in rod shape with a diameter of 500 µm, and the chemical composition is listed in Table 1. The rod was fixed vertically so that the laser irradiated at the end, as shown in Figure 1. After passing through a collimating system and a deflection unit (AXIALSCAN-30, RAYLASE GmbH), laser beam was laterally focused on the end of the rod, with a spot diameter of 55 µm. With a constant scan track of 5 mm, preforms were generated with different processing parameter. Laser power was adjusted to 30 W, 60 W and 90 W, and three different scanning speeds for each laser power was used, in which a spherical preform could be generated successfully. Based on this, each parameter combination was repeated three times. Argon was used as shielding gas.

Table 1: Chemical composition of the used Nitinol [13]

	Ni	C	O	Fe	other	Ti
wt%	55.5	≤0.05	≤0.05	≤0.05	<0.01	bal.

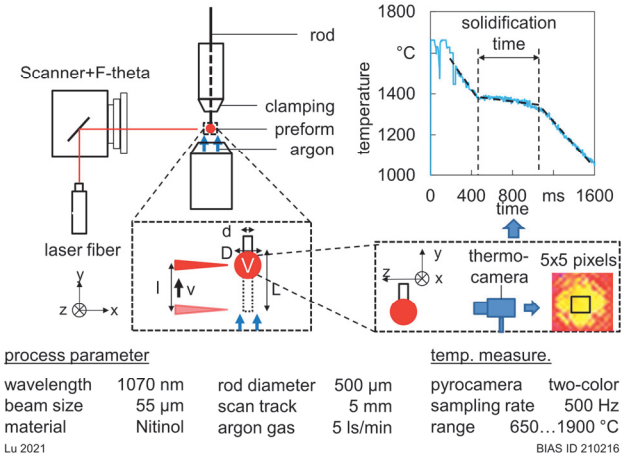

Figure 1: Scheme of laser rod end melting of Nitinol with online temperature monitoring

2.2. Temperature measurement and analysis

During the laser rod end melting, transient temperature distribution of the accumulating preform was recorded by a quotient thermal camera (HDRC@-Q-PyroCam GigE, IMS CHIPS Stuttgart) at the sampling rate of 500 Hz, and the measuring direction is shown in Figure 1. This thermal camera compares the signal at the wavelength of 661 nm and 667 nm between 650 °C and 1900 °C. To minimize the background noise, a notch filter (TECHSPEC OD 6.0, Edmund Optics GmbH) was amounted in front of the thermal camera, so that the signal of laser source at 1070 nm was attenuated almost completely. In addition, the experiment was conducted in the dark environment to avoid the background light noise.

Based on a LabView based evaluation algorithm [14], temperature signals of the generated preform during the cooling process were analyzed, where 5×5 pixels were extracted from the region of the preform to calculate mean surface temperature at each sampling time. This mean temperature was regarded as the global temperature of preform. The obtained temperature time distribution of the preform was further used to calculate the global solidification time, which indicated the time interval between liquidus and solidus of the Nitinol. Specifically, the liquidus and solidus temperature was recognized as the start and end point of quasi-plateau from the temperature time course. Then the global solidification time was obtained by determining the two intersections of three linear regressions (melt, mushy zone and solidified preform) in this region, as shown in Figure 1.

2.3. Analysis methods for preform

The generated preforms were characterized in terms of geometry, surface topography and microstructure. Assuming that the preform had a perfect spherical shape, by means of a micrometer screw gauge, mean diameter D of the preform was determined based on five measurements for each specimen. Afterwards, the surface topography of the preform was characterized by an optical microscope with digital depth composition function (VHX-1000, KEYENCE Deutschland GmbH). Then longitudinal section of specimen was embedded, polished and etched with Kroll solution (93 mL H_2O, 5 mL HNO_3 and 2 mL HF) for about 2 mins, so that the microstructure of Nitinol preforms as well as the heat affected zone in the rod was identified.

Specimens were further characterized by an X-ray computed tomography (CT) scanner (Phoenix-xray v|tome|x m, GE Sensing & Inspection Technologies GmbH) to analyze pores and their spatial distribution. This machine worked at voltage of 180 kV and enabled spatial resolution of 1.7 µm.

3. Results

3.1. Geometry and surface quality

Figure 2 shows the diameter of the Nitinol preform. For the same laser power, with increasing scan rate, preform diameter increased firstly and then decreased. In addition, the diameter of preform showed an increasing tendency with increasing laser power, which led to a larger

processing window for the scan rate. As the scan rate differs larger, more apparent difference in solidification and surface quality is expected. Therefore, the further study regarding the surface quality and microstructure is based on the laser power of 90 W.

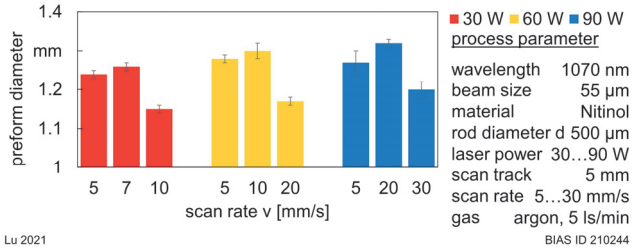

Figure 2: Diameter of Nitinol preforms

Figure 3 presents the surface quality of preforms with different parameter sets. With the minimum available scan rate, from the end of the wire there was striped structure, followed with comb structure to the end of the preform. As an intermediate scan rate was applied, the whole surface was comparatively smooth. With higher scan rate, the striped structure and comb structure re-appeared, along with a dense distribution of micro dots at the end of the preform.

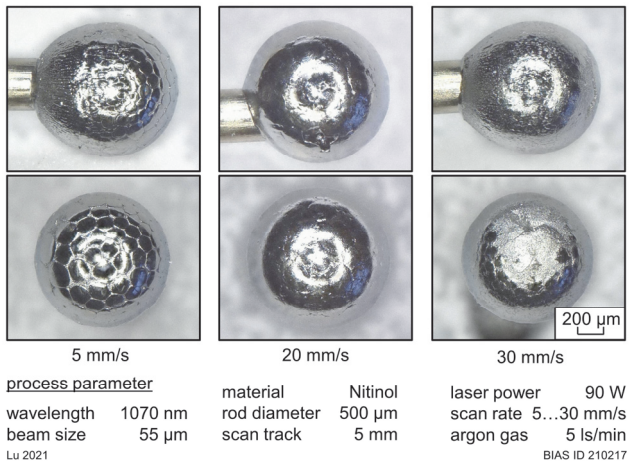

Figure 3: Surface quality of Nitinol preforms

The possible defects were determined in the X-ray CT scanning of the preform, as shown in Figure 4. The side view shows one slice of cross-section with a void and the top view indicates that this void was opened at the surface of preform end. Near the void entrance cracks were generated. These similar defects were found for all studied specimens. Besides the large void, micro pores (blue points in Figure 4) with volume under 500 µm^3 distributed randomly in the preform.

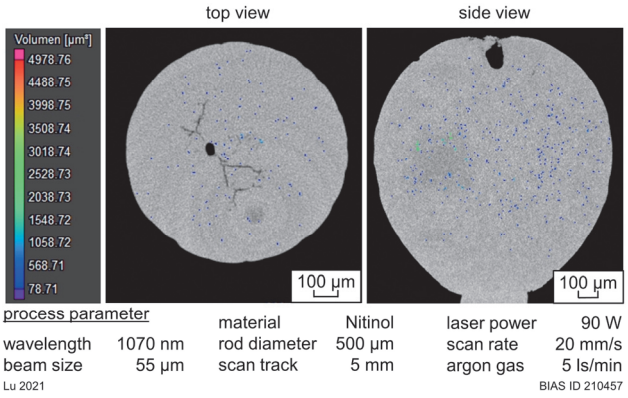

Figure 4: Defects of the Nitinol preform measured by X-ray CT scanner

3.2. Solidification time and microstructure

Figure 5 shows three different zones (marked with A, B and C) in the preform generated by the scan rate of 5 mm/s. The transition zones are shown with higher magnification in Figure 6. Zone A was the heat affected zone of the wire, followed by columnar dendrites in Zone B with grain orientation perpendicular to the fusion line. The Zone B was further surrounded with Zone C consisting of several large grains, in which typical columnar dendrites were identified. These grains were orientated perpendicular to the surface and grew towards the boundary between Zone B and Zone C, where finer microstructure compared to the elsewhere in Zone C was found. In addition, it was found that the dendrites were courser in Zone C than in Zone B. The Zone C was covered by a thin surface layer with planar structure, separated by several micro dimples (cf. Figure 6 left). It took about 600 ms to solidify from complete liquid state to complete solid state at the surface.

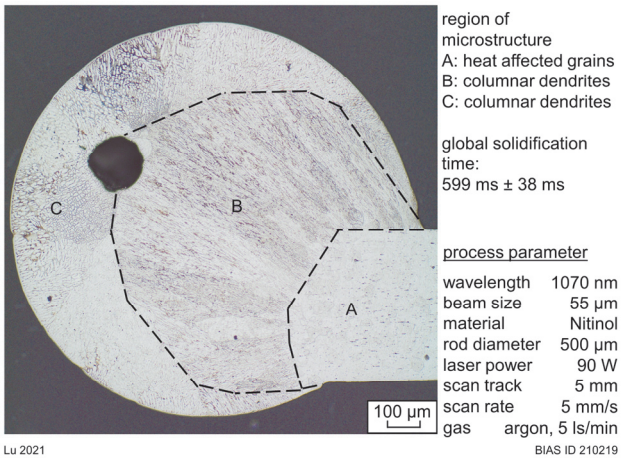

Figure 5: Microstructure of Nitinol preform with scan rate of 5 mm/s

As the scan rate of 20 mm/s was applied, besides the typical zones and corresponding microstructure observed in Figure 5, additional Zone D was found in Figure 7. The Zone D consisted of coarse column-shaped grains. Compared to the Zone C in Figure 5, there was no

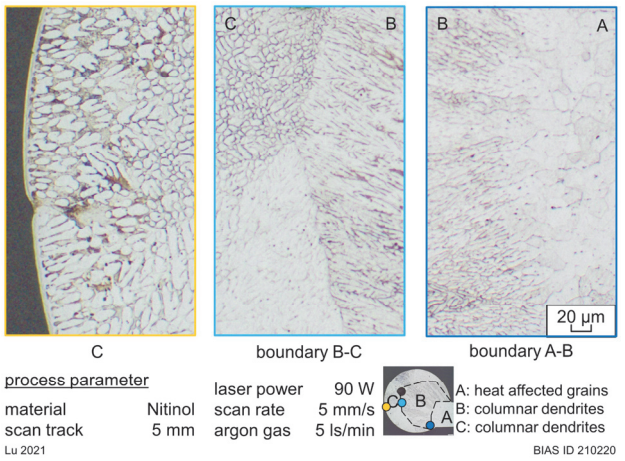

Figure 6: Transition zones in the Nitinol preform with scan rate of 5 mm/s

thin surface layer with planar microstructure and no grain in Zone C with dimples at the surface was observed, as shown in Figure 8. The global solidification time at the surface is around 644 ms, slightly larger than that for the scan rate of 5 mm/s and 30 mm/s.

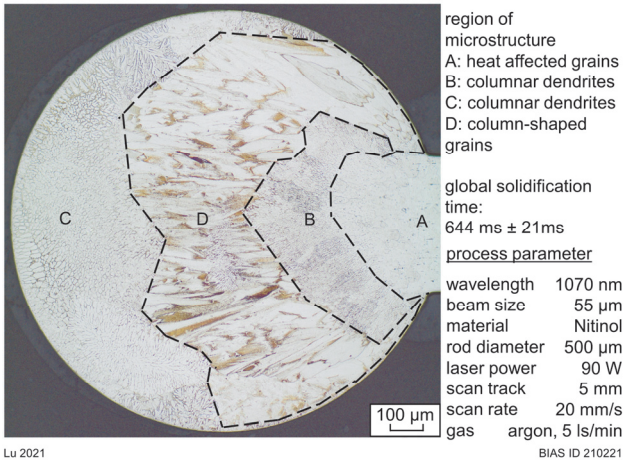

Figure 7: Microstructure of Nitinol preform with scan rate of 20 mm/s

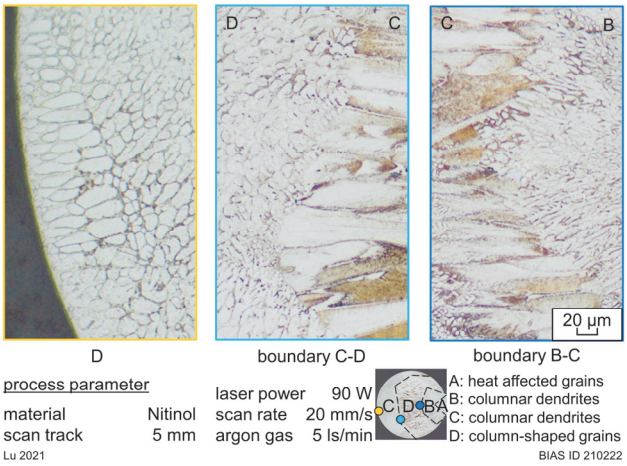

Figure 8: Transition zones in the Nitinol preform with scan rate of 20 mm/s

When the scan rate increased to 30 mm/s, the Zone D in Figure 7 was not identified (cf. Figure 9), and the microstructure distribution and grain orientation was comparable to the scan rate of 5 mm/s. Furthermore, surface layer with planar microstructure was identified again, while some dendritic structure could be observed at the surface of the end of preform (cf. Figure 10 left). The global solidification time of about 600 ms was comparable to that for the scan rate of 5 mm/s.

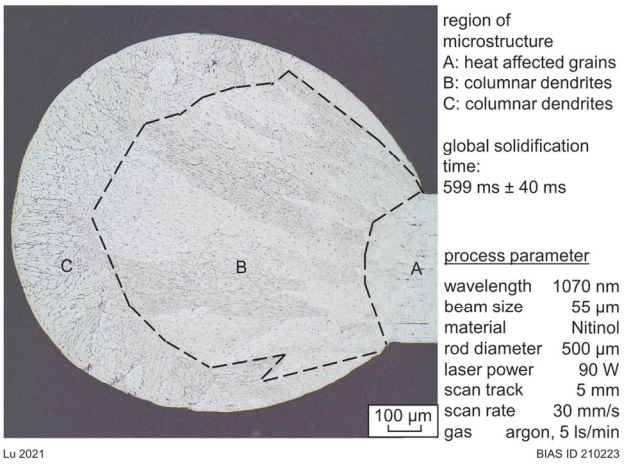

Figure 9: Microstructure of Nitinol preform with scan rate of 30 mm/s

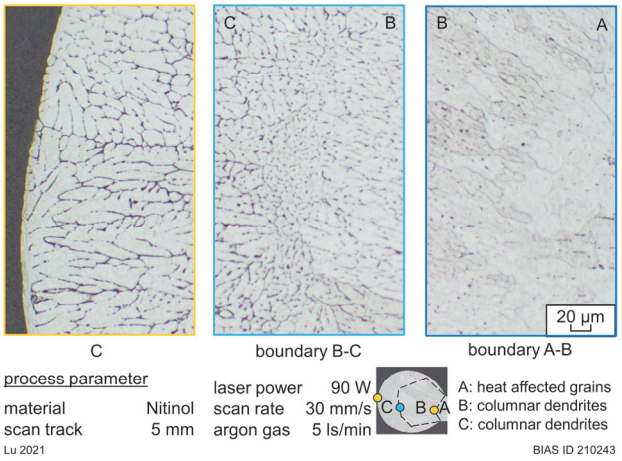

Figure 10: Local enlargement of microstructure in the Nitinol preform with scan rate of 30 mm/s

4. Discussion

The results showed that the laser parameter influenced the final geometry, microstructure and surface quality. Thereby, the occurrence of pores and cracks have to be taken into account. As the scan rate increased, the preform diameter increased slightly first and then decreased. The decrease of the preform diameter and volume should be explained by the insufficient energy coupling to the accumulated melt [5]. In addition, it was shown in the literature that in the laser rod end melting radiation dominates the heat dissipation more than heat conduction and convection at the surface during the cooling process [4]. The solidification process should thereby start at the surface of the preform and at the connection between the fusion zone and the heat affected wire. Based on the observed grain orientation, two solid fronts encountered at the boundary of Zone B

and Zone C for the scan rate of 5 mm/s and 30 mm/s, and at the boundary of Zone C and Zone D for 20 mm/s.

Preform with different scan rates contained different microstructures. As introduced, the solidified microstructure in the FZ is mainly determined by the temperature gradient and growth rate [8]. This microstructure affects the surface appearance. Comparison of the surface with the microstructure shows clearly that the grains (cf. Figure 3, Figure 5 and Figure 9) and further the (secondary) dendrites lead to the different shown surface structures (cf. Figure 3 and Figure 10). These findings are in line with the results shown in [15] where the occurrence of surface structures due to secondary dendrite arms in case of laser rod end melting of AISI 304 are shown. These findings show therefore that laser rod end melting can principally be applied on Nitinol to generate preforms for flanges whereby the surface quality depends significantly on the solidification conditions.

5. Conclusion

It was shown that the laser rod end melting can be principally applied on Nitinol to generate preforms for flanges. Herby defects of voids, cracks and pores have to be taken into account. Thereby, the scan rate determines the solidification condition, leading to four typical microstructure zones with columnar dendrites and column-like grains. These microstructure leads to different surface structures. Hence, the solidification conditions significantly determine the surface quality.

Acknowledgement

The authors gratefully acknowledge the financial support for the project “Laserschmelzen im Gesenk” funded by the Deutsche Forschungsgemeinschaft (DFG, German Research Foundation) – Projektnummer 449377606. In addition, a grateful appreciation is given to Mr. Dieter Tyralla for the self-writing LabVIEW programs and Mr. Christian Kapitza for the operation of X-ray CT scanner.

References

[1] Velmurugan, C.; Senthilkumar, V., et al. 2018. Machining of NiTi-shape memory alloys-A review. Machining Science and Technology. 22. pp. 355–401.

[2] Mertmann, M.; Vergani, G. 2008. Design and application of shape memory actuators. The European Physical Journal Special Topics. 158. pp. 221–230.

[3] Mehrpouya, M.; Gisario, A., et al. 2021. Laser welding of nickel-titanium (NiTi) shape memory alloys(Eds.), Advanced Welding and Deforming. Elsevier. pp. 203–230.

[4] Vollertsen, F.; Friedrich, S., et al. 2020. Cold Micro Metal Forming. Springer International Publishing. Cham.

[5] Brüning, H. 2016. Prozesscharakteristiken des thermischen Stoffanhäufens in der Mikrofertigung.

[6] Stephen, A.; Vollertsen, F. 2010. Upset ratios in laser-based free form heading. Physics Procedia. 5. pp. 227–232.

[7] Oliveira, J.; Miranda, R.; Braz Fernandes, F. 2017. Welding and Joining of NiTi Shape Memory Alloys: A Review. Progress in Materials Science. 88. pp. 412–466.

[8] Kou, S. 2002. Welding Metallurgy (Second Edition). Wiley-Interscience. S.l.

[9] Mehrpouya, M.; Gisario, A., et al. 2018. Laser welding of NiTi shape memory sheets using a diode laser. Optics & Laser Technology. 108. pp. 142–149.

[10] Vieira, L.; Fernandes, F., et al. 2011. Mechanical behaviour of Nd:YAG laser welded superelastic NiTi. Materials Science and Engineering: A. 528. pp. 5560–5565.

[11] Song, Y.; Li, W., et al. 2008. The influence of laser welding parameters on the microstructure and mechanical property of the as-jointed NiTi alloy wires. Materials Letters. 62. pp. 2325–2328.

[12] Panton, B. 2016. Laser Processing, Thermomechanical Processing, and Thermomechanical Fatigue of NiTi Shape Memory Alloys.

[13] SAES Group. Brochure SAES Smart Materials. https://www.saesgetters.com/brochure-saes-smart-materials (accessed 2021.06.15).

[14] Tyralla, D.; Seefeld, T. 2021. Thermal Based Process Monitoring for Laser Powder Bed Fusion (LPBF). Advanced Materials Research. 1161. pp. 123–130.

[15] Brüning, H.; Teepe, M.; Vollertsen, F. 2014. Surface Roughness and Size Effect in Dendrite Arm Spacing at Preforms of AISI 304 (1.4301) Generated by Laser Rod End Melting. Procedia Engineering. 81. pp. 1589–1594.